RSC Advances

PAPER

View Article Online
View Journal | View Issue

Cite this: *RSC Adv.*, 2021, **11**, 38814

The interesting luminescence behavior and rare nonlinear optical properties of the {$Ag_{55}Mo_6$} nanocluster†

Kun Zhou,[ab] Li-Kai Yan,[a] Yun Geng,*[a] Jiu-Yu Ji,[b] Xin-Long Wang,*[a] Zhong-Min Su[a] and Zheng-Guo Xiao*[c]

Received 1st September 2021
Accepted 30th November 2021

DOI: 10.1039/d1ra06569f

rsc.li/rsc-advances

The remarkably reversible thermochromic luminescence behavior and the rare nonlinear optical (NLO) properties of the $[Ag_{55}(MoO_4)_6(C{\equiv}C^tBu)_{24}(CH_3COO)_{18}(CH_3COO)]\cdot 2H_2O$ ({$Ag_{55}Mo_6$} for short) nanocluster reported were investigated experimentally. The important contributions of Ag^+, $C{\equiv}C^-$ ions and MoO_4^{2-} groups to the NLO properties were proved by further density functional theory (DFT) calculations.

Research into high-nuclearity transition-metal clusters has become increasingly intensive due to their fascinating structures and extensive applications.[1,2] As for high-nuclearity silver clusters, although many wonderful structures have been discovered, studies of their properties are very few. Therefore, to maximize application of high-nuclearity silver clusters, the research of their physical/chemical properties is highly desirable.[3,4]

On one hand, studying luminescence properties of high-nuclearity silver clusters has great scientific significance to the development of smart optical materials. In recent years, research on the luminescence property of high-nuclearity silver clusters has been actively pursued because of their numerous potential applications in light emitting devices.[5,6] As far as we know, silver chalcogenolate clusters have excellent luminescence properties.[7] Wang, Zang and Sun *et al.* have reported some temperature-sensitive luminescent silver chalcogenolate clusters, which emit weak lights at room temperature while emit bright lights at 77 K.[6,8] For example, a polyoxometallate (POM for short) functionalized multiple core–shell Ag_{84} nanocluster $[Ag_{10}@(W_7O_{26})_2@Ag_{74}S_2(^i\text{PrS})_{40}(n\text{PrCOO})_{18}]\cdot 2CH_3OH$ shows the temperature-dependent emission property.[6] Recently, Zang and Sun *et al.* have reported turn-on luminescence[9] and aggregation-induced emission in silver chalcogenolate cluster metal–organic frameworks/gels.[10] However, there is very little research on the luminescence property of high-nuclearity silver alkynyl clusters.[11] Firstly, a new silver alkynyl nanocluster $[Ag_{42}\{Eu(W_5O_{18})_2\}(^t\text{BuC}{\equiv}\text{C})_{28}Cl_4][OH]\cdot H_2O$ has been reported by Gao, and this compound exhibits an unusual fluorescence enhancement superior to the polyoxoanionic $[Eu(W_5O_{18})_2]^{9-}$ precursor.[12] Besides, Wang *et al.* have reported two unprecedented solution-stable silver alkynyl clusters, $[Ag_7(C_2)(CF_3CO_2)_5(bpy)_5]\cdot MeCN\cdot 0.5MeOH$ and $[Ag_7(C_2)(CF_3CO_2)_5(phen)_5]\cdot 2CH_2Cl_2$. Both of the two compounds are not emissive at room temperature, while the frozen glasses of them (MeCN/MeOH, 1 : 1) are luminescent at 77 K.[13] A novel silver-alkynyl cluster based NbO-type framework $[Cl@Ag_{18}(c\text{PrC}{\equiv}\text{C})_{17}BF_4]n$ showing unprecedented triple emission spanning from the visible to near-infrared (NIR) region has been reported by Sun.[14] The above studies provide positive guidance for the luminescence exploration of silver alkynyl clusters.

On the other hand, studying the nonlinear optical (NLO) properties of silver alkynyl clusters also has great scientific significations to the development of smart optical materials. It is well known that NLO materials with abundant delocalized π electrons and ultrafast NLO response act as an important role in optoelectronic technologies and all-optical switch regions, thus much attention has been focused on investigate the NLO responses of metal clusters. Metal ions and organic ligands have been proved to be two important factors for the NLO original mechanism of metal clusters.[15,16] The reason why metal clusters have large third-order NLO properties is that more electronic transitions can be allowed to take place after heavy-metal ions introduction.[17] In silver alkynyl clusters with heavy-metal silver involved, d–pπ delocalized and d–dπ conjugated characteristics of alkynyl ligand make them serve as excellent NLO materials.[18,19] Currently, although the NLO properties of many metal clusters have been studied, but there are few studies on the NLO properties of silver clusters.[19–23] Given this, it

[a]*Institute of Functional Material Chemistry, Faculty of Chemistry, Northeast Normal University, Changchun 130024, Jilin, China. E-mail: gengy575@nenu.edu.cn; wangxl824@nenu.edu.cn*

[b]*School of Petrochemical Engineering, Liaoning Petrochemical University, Fushun 113001, Liaoning, China*

[c]*Department of Physics and Electronic Engineering, Tongren University, Tongren 554300, Guizhou, China. E-mail: xiangyunonlinear@gmail.com*

† Electronic supplementary information (ESI) available: Details of experimental and physical measurements. See DOI: 10.1039/d1ra06569f

is essential to explore the relationship of structures and NLO properties of high-nuclearity silver alkynyl nanoclusters.

The ultrastable $[Ag_{55}(MoO_4)_6(C{\equiv}C^tBu)_{24}(CH_3COO)_{18}\text{-}(CH_3COO)]\cdot 2H_2O$ ($\{Ag_{55}Mo_6\}$) silver alkynyl nanocluster possessing a Ag-centered multishell structure has been chemically well-defined and characterized by our group in 2014.[24] In this paper, we will focus on the optical properties of the $\{Ag_{55}Mo_6\}$ nanocluster. Luminescence spectra of the $\{Ag_{55}Mo_6\}$ nanocluster from 298 K to 77 K were measured. The results indicate that the $\{Ag_{55}Mo_6\}$ nanocluster presents reversible thermochromic luminescence behavior, which is rare in the known inorganic–organic silver alkynyl hybrids. And the NLO property of the $\{Ag_{55}Mo_6\}$ nanocluster was investigated by femtosecond Z-scan technique and its molecular frontier orbitals were simulated by quantum chemical methods. These results indicate $\{Ag_{55}Mo_6\}$ has a good application prospect for fluorescent probe and NLO materials.

Luminescence property

Luminescence property of the $\{Ag_{55}Mo_6\}$ nanocluster in the solid state was investigated by an F-4500 Fluorescence (FL) Spectrophotometer. It shows a maximum emission peak at 439 nm accompanied by a shoulder peak at 418 nm upon the excitation wavelength of 365 nm at 298 K (Fig. 1a, violet trace). The short lifetime of the maximum emission at 439 nm was measured to be ~14.0 ns, suggesting the emission is fluorescence. The quantum efficiency of the photoluminescence is ~0.1%. Interestingly, it also emits orange light at 77 K, exhibiting a maximum emission peak at 608 nm upon the excitation wavelength of 365 nm (Fig. 1a, orange trace). By comparing the two emission spectra at 298 K and at 77 K, it can be found that the intensity of the emission peak at 608 nm gradually increases while the emission peak at 439 nm gradually weakens as the temperature decreases from 298 K to 77 K (Fig. 1a and S1†). To investigate the change of emission peak intensity at 608 nm, temperature dependent luminescence spectra of the $\{Ag_{55}Mo_6\}$ nanocluster were recorded at 298, 255, 173, 130 and 77 K by a combined fluorescence lifetime and steady state spectrometer FLSP920. The maximum emission band of the $\{Ag_{55}Mo_6\}$ nanocluster at 608 nm was still kept upon a series of excitation wavelengths (365 nm, 378 nm, 421 nm and 467 nm) at low temperature. As shown in Fig. 1 and S2,† the emission peak intensity of the $\{Ag_{55}Mo_6\}$ nanocluster at 608 nm stepwise increases upon excitation at 421 nm when the temperature cooling from 298 to 77 K. To explore the luminescence mechanism of the $\{Ag_{55}Mo_6\}$ nanocluster, luminescence properties of $AgC{\equiv}C^tBu$ ligand and the mixture of initial reaction materials were investigated. As shown in Fig. S3 and S4,† at both 298 K and 77 K, no emission peaks around 608 nm were detected from their luminescence spectra, and not to mention intensity. Therefore, we infer the thermochromic luminescence behavior of the $\{Ag_{55}Mo_6\}$ nanocluster should be assigned to the characteristic of the $\{Ag_{55}Mo_6\}$ nanocluster. With reference to the spectra of related silver clusters,[25] the emission of the $\{Ag_{55}Mo_6\}$ nanocluster at 298 K should be a ligand-to-metal-charge-transfer (LMCT) transition combined with the cluster-centered (CC) transition disturbed by Ag···Ag interactions. While the emission of the $\{Ag_{55}Mo_6\}$ nanocluster at low temperature should be attributable to the CC excited state. Ag···Ag distance thermal compression occurred in the $\{Ag_{55}Mo_6\}$ nanocluster leading to enhanced rigidity and faster intersystem crossing process as the temperature decreases, effectively reducing the energy loss of non-radiation decay. As a result, the CC emission stepwise strengthens from 298 to 77 K. The thermochromic luminescence behavior of the $\{Ag_{55}Mo_6\}$ nanocluster is reversible between 298 and 77 K. As well as known, fluorescence of POMs is very weak. Surprisingly, the $\{Ag_{55}Mo_6\}$ nanocluster embedded by six MoO_4^{2-} POM building units possesses such an excellent luminescence behavior, which is rare in the known inorganic–organic silver alkynyl hybrids. Owing to its eye-detected temperature-sensitive emission, the $\{Ag_{55}Mo_6\}$ nanocluster has great potential for light-emitting materials, sensor for temperatures and temperature probes.

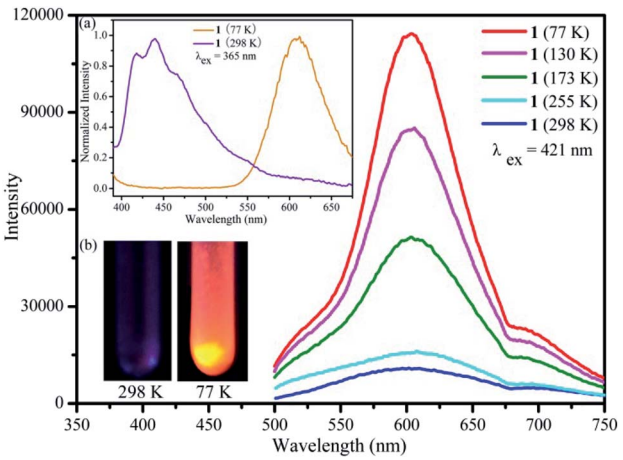

Fig. 1 Emission spectra of the $\{Ag_{55}Mo_6\}$ nanocluster at different temperatures upon excitation at 421 nm. Inset (a) emission (violet trace) and (orange trace) spectra of the $\{Ag_{55}Mo_6\}$ nanocluster at 298 and 77 K upon excitation at 365 nm; (b) luminescence photographs of the $\{Ag_{55}Mo_6\}$ nanocluster at 298 and 77 K excited with a hand-held UV lamp (365 nm).

Third-order nonlinear optical property

The linear absorption spectrum of the $\{Ag_{55}Mo_6\}$ nanocluster in CH_3OH solution is presented in Fig. 2. While the excitation

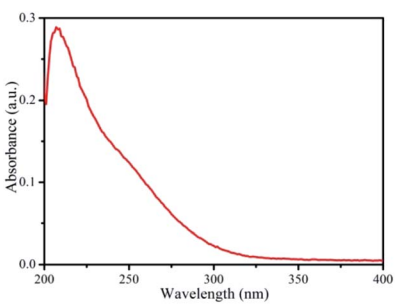

Fig. 2 Absorption spectrum of the $\{Ag_{55}Mo_6\}$ nanocluster in CH_3OH solution.

wavelength of the laser light is 400 nm, which satisfies the non-resonant absorption condition in Z-scan measurement.[26]

The third-order NLO property of the $\{Ag_{55}Mo_6\}$ nanocluster with the concentration of 9.0×10^{-5} mol L^{-1} was investigated under 190 fs laser pulses with the wavelength of 400 nm. Z-scan data (open-aperture and closed aperture data) of the $\{Ag_{55}Mo_6\}$ nanocluster dissolved in the CH_3OH solution are shown in Fig. 3. The results indicate that the $\{Ag_{55}Mo_6\}$ nanocluster shows very strong NLO responses included nonlinear absorptive and refractive effects. The nonlinear absorption component was evaluated by open-aperture Z-scan (Fig. 3a). The open-aperture Z-scan experimental data of the $\{Ag_{55}Mo_6\}$ nanocluster can be well described by eqn (1) and (2),[27] which can also explain the nonlinear absorption process:

$$T(z) = \frac{1}{\sqrt{\pi}q(z)} \int_{-\infty}^{\infty} \ln\left[1 + q(z)e^{-t^2}\right] dt \quad (1)$$

$$q(z) = \int_{-\infty}^{\infty} \int_{0}^{\infty} \beta \frac{I_0}{1 + (Z/Z_0)^2} e^{\left(-2(r/\omega_0)^2 - (t/t_0)^2\right)} \frac{1 - e^{-\alpha_0 L}}{\alpha_0} r dr dt \quad (2)$$

where light transmittance T represents a function of the sample's Z-position (with respect to focal point $z = 0$), I_0 represents the peak irradiation intensity at focus, L represents the sample thickness, z represents the distance of the sample from the focal point, $z_0 = \pi\omega_0^2/\lambda$ (where ω_0 represents the spot radius of the laser pulse at focus and λ represents the laser wavelength), t represents the time, t_0 represents the pulse width, r represents the radial coordinate, α_0 and β represent linear absorption coefficient and effective third-order NLO absorptive coefficient, respectively. In Fig. 3a, it is clear to be observed that the normalized transmittance of the $\{Ag_{55}Mo_6\}$ nanocluster decreases when it is brought closer to the focal point ($z = 0$). It suggests that the $\{Ag_{55}Mo_6\}$ nanocluster exhibits strong reverse saturable absorption (RSA). Moreover, the NLO absorptive coefficient (β) of the $\{Ag_{55}Mo_6\}$ nanocluster was calculated to be 6.2×10^{-12} m^2 W^{-1} through curve fitting, shown in Fig. 3a. As for NLO refractive effect, the $\{Ag_{55}Mo_6\}$ nanocluster performed large self-focusing effect for valley-peak configuration, shown in Fig. 3b.

In addition, in order to eliminate the nonlinear refraction of solvent CH_3OH, the nonlinear refraction Z-scan curve of solvent CH_3OH shown in Fig. 4 was carried out under the same experimental condition with the one of $\{Ag_{55}Mo_6\}$ nanocluster performed in Fig. 3a. From Fig. 4, the solvent CH_3OH also performed nonlinear refraction effect. As a result, when considering the pure NLO effect of $\{Ag_{55}Mo_6\}$ nanocluster, the NLO effect of solvent CH_3OH should be subtracted. An effective third-order NLO refractive index n_2 of the $\{Ag_{55}Mo_6\}$ nanocluster can be obtained from the difference between the normalized transmittance values at the valley and peak positions (ΔT_{V-P}) using eqn (3),[27]

$$n_2 = \frac{\lambda\alpha_0}{0.812\ \pi I(1 - e^{-\alpha_0 L})} \Delta T_{V-P} \quad (3)$$

where I represents the light intensity of incident pulse, and λ represents the wavelength of the laser. The NLO refractive indices (n_2) of the $\{Ag_{55}Mo_6\}$ nanocluster solution and solvent CH_3OH were estimated to be 3.7×10^{-19} m^2 W^{-1} and 1.1×10^{-19} m^2 W^{-1} through curve fitting, respectively. Then the pure NLO refractive index (n_2) of the $\{Ag_{55}Mo_6\}$ nanocluster was estimated to be 2.6×10^{-19} m^2 W^{-1}.

The real and imaginary parts of $\chi^{(3)}$ of the $\{Ag_{55}Mo_6\}$ nanocluster can be obtained by eqn (4) and (5):[28]

$$\mathrm{Re}\chi^{(3)} = cn_0 2n_2/120\pi^2 \quad (4)$$

$$\mathrm{Im}\chi^{(3)} = c^2 n_0 2\beta/240\pi^2\omega \quad (5)$$

Thus, the coefficient of the effective third-order susceptibility $\chi^{(3)}$ was 1.63×10^{-13} esu.

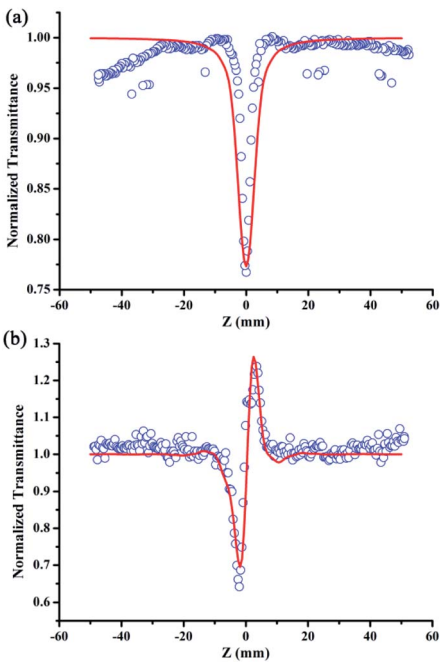

Fig. 3 Z-scan measurement of the $\{Ag_{55}Mo_6\}$ nanocluster in CH_3OH solution at 400 nm with the linear transmittance of 60% at 13 μJ pulse: (a) data collected under the open-aperture configuration. (b) Data obtained by dividing the normalized Z-scan data obtained under the closed-aperture configuration by the normalized Z-scan data in (a). Solid lines represent theoretical fits.

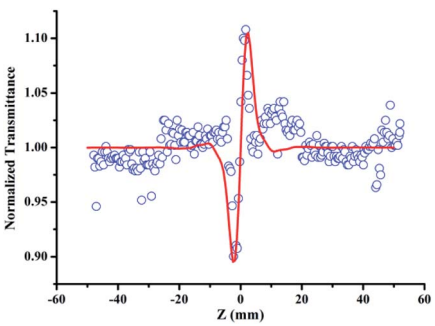

Fig. 4 Data collected under the closed-aperture configuration of CH_3OH solution at 400 nm with the linear transmittance of 60% at 13 μJ pulse. Solid lines represent theoretical fits.

The corresponding coefficient of the hyper-polarizability γ can be calculated by the following eqn (6),[29]

$$\chi^{(3)} = \gamma N F^4 \quad (6)$$

where N represents the number density of the $\{Ag_{55}Mo_6\}$ nanocluster in the sample solution, is the local field correction factor and the n_0 represents the refractive index of the solvent. Thus, the coefficient of the hyper-polarizability γ is determined to be 1.22×10^{-30} esu, which is comparable to silver clusters and other metal complexes,[19–23,30–34] indicating it can be used for the application of NLO domain.

Density functional theory (DFT) calculations

To further explore the origin of the third-order NLO property, the electronic structures of the $\{Ag_{55}Mo_6\}$ nanocluster were simultaneously investigated *via* theoretical calculations (Fig. 5).

This $\{Ag_{55}Mo_6\}$ nanocluster is so large that it is difficult to give a common simulation using density functional theory (DFT), thereby we employed the typical functional B3LYP, 3-21G basis set for non-metal atoms and LAND2DZ basis set for Ag and Mo atoms to carry out single-point calculation in order to obtain the electronic structures.[35] The frontier molecular orbitals including the highest occupied molecular orbital (HOMO), HOMO−1, HOMO−2, the lowest unoccupied molecular orbital (LUMO), LUMO+1 and LUMO+2 are shown in Fig. 5. Obviously, the occupied molecular orbitals mainly distribute at $C{\equiv}C^-$ and Ag^+ ions, while the unoccupied molecular orbitals are mainly localized at MoO_4^{2-} groups, which suggest the obvious charge transfer characterization when this nanocluster is excited by the photon. As we all know it, the charge transfer is favourable for the NLO response, thus it can be determined that the contribution of the Ag^+ and $C{\equiv}C^-$ ions and the MoO_4^{2-} groups to the NLO property of the $\{Ag_{55}Mo_6\}$ nanocluster by molecular orbital theory. Therefore, we can deduce that the NLO property of the $\{Ag_{55}Mo_6\}$ nanocluster is controlled by the $Ag_{55}Mo_6$ and $C{\equiv}C^-$ ions. This finding is consistent with the experimental results: the $\{Ag_{55}Mo_6\}$ nanocluster performs strong reverse saturable absorption (RSA) and self-focusing nonlinear refractive effect in our Z-scan measurements. The observed NLO effect can be attributed to the two-photon absorption (TPA) and the excited-state absorption induced by TPA in this case.[16,36]

An ideal optical limiting (OL) material should have these characteristics: the ability of responding quickly to the incident light and increasing opaque as the light intensity increases. The $\{Ag_{55}Mo_6\}$ nanocluster displays such an OL ability for the ultrafast strong NLO response and showing transparent under low light intensity.

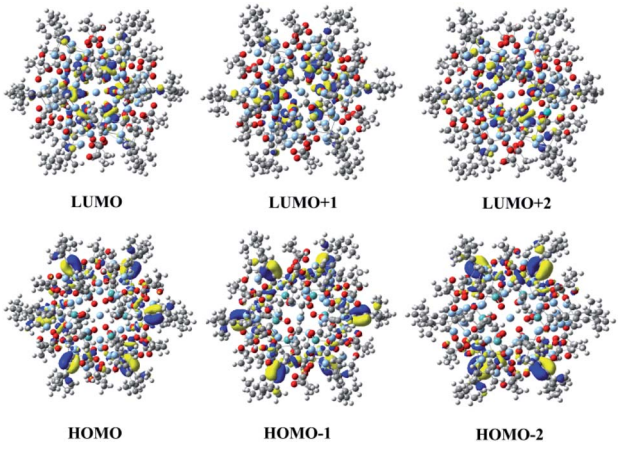

Fig. 5 The frontier molecular orbitals including HOMO−2, HOMO−1, HOMO, LUMO, LUMO+1 and LUMO+2 of the $[Ag_{55}(MoO_4)_6(C{\equiv}C^tBu)_{24}(CH_3COO)_{18}]^+$ cluster skeleton in the $\{Ag_{55}Mo_6\}$ nanocluster.

Conclusion

In summary, the optical properties of the chemically well-defined $\{Ag_{55}Mo_6\}$ nanocluster were investigated. Surprisingly, the $\{Ag_{55}Mo_6\}$ nanocluster presents reversible thermochromic luminescence behavior, which is rare in the known inorganic–organic silver alkynyl hybrids. Moreover, the third-order NLO properties of the $\{Ag_{55}Mo_6\}$ nanocluster have been studied by using the Z-scan technique at 400 nm with 190 fs laser pulses, and the results show the $\{Ag_{55}Mo_6\}$ nanocluster displays strong reverse saturable absorption and its second-order hyper-polarizability γ is estimated to be 1.22×10^{-30} esu. The DFT calculations suggest the important contribution of $Ag_{55}Mo_6$ and $C{\equiv}C^-$ ions to the NLO properties. These results indicate that the $\{Ag_{55}Mo_6\}$ nanocluster has great potential in light emitting devices and ultrafast optical limiter in the near future.

Conflicts of interest

There are no conflicts to declare.

Acknowledgements

This work was supported financially by the 61st batch of China Postdoctoral Science Foundation (No. 415-111900347), the NSFC of China (No. 21671034, 21771035), the Education Department of Liaoning Province Youth Project (No. L2020039), Science and Technology Foundation of Tongren City (Grant No. [2017] 47-37), Startup Foundation for Doctoral Research (trxyDH1622) and Science and Technology Foundation of Guizhou Province Education Department (Grant No. KY[2018]343).

Notes and references

1 (*a*) A. V. Anyushin, A. Kondinski and T. N. Parac-Vogt, *Chem. Soc. Rev.*, 2020, **49**, 382–432; (*b*) S. K. Langley, R. A. Stott, N. F. Chilton, B. Moubaraki and K. S. Murray, *Chem. Commun.*, 2011, **47**, 6281–6283; (*c*) X.-J. Kong, L.-S. Long, Z.-P. Zheng, R.-B. Huang and L.-S. Zheng, *Acc. Chem. Res.*, 2010, **43**, 201–209; (*d*) G. E. Kostakis and A. K. Powell, *Coord. Chem. Rev.*, 2009, **253**, 2686–2697; (*e*) G. Mezei,

C. M. Zaleski and V. L. Pecoraro, *Chem. Rev.*, 2007, **107**, 4933–5003; (*f*) S. Horiuchi, S. Moon, A. Ito, J. Tessarolo, E. Sakuda, Y. Arikawa, G. H. Clever and K. Umakoshi, *Angew. Chem., Int. Ed.*, 2021, **60**, 10654–10660.

2 (*a*) R. J. Wilson, N. Lichtenberger, B. Weinert and S. Dehnen, *Chem. Rev.*, 2019, **119**, 8506–8554; (*b*) X.-Y. Zheng, J. Xie, X.-J. Kong, L.-S. Long and L.-S. Zheng, *Coord. Chem. Rev.*, 2019, **378**, 222–236; (*c*) C. Papatriantafyllopoulou, E. E. Moushi, G. Christou and A. J. Tasiopoulos, *Chem. Soc. Rev.*, 2016, **45**, 1597–1628; (*d*) X. K. Fang, L. Hansen, F. Haso, P. C. Yin, A. Pandey, L. Engelhardt, I. Slowing, T. Li, T. B. Liu, M. Luban and D. C. Johnston, *Angew. Chem., Int. Ed.*, 2013, **52**, 10500–10504; (*e*) G. E. Kostakis, S. P. Perlepes, V. A. Blatov, D. M. Proserpio and A. K. Powell, *Coord. Chem. Rev.*, 2012, **256**, 1246–1278.

3 (*a*) J. A. Chipman and J. F. Berry, *Chem. Rev.*, 2020, **120**, 2409–2447; (*b*) S.-Q. Zhang and L. Zhao, *Acc. Chem. Res.*, 2018, **51**, 2535–2545; (*c*) J.-Z. Yan, B. K. Teo and N.-F. Zheng, *Acc. Chem. Res.*, 2018, **51**, 3084–3093; (*d*) A. Ghosh, O. F. Mohammed and O. M. Bakr, *Acc. Chem. Res.*, 2018, **51**, 3094–3103; (*e*) Z. Lei, X.-K. Wan, S.-F. Yuan, Z.-J. Guan and Q.-M. Wang, *Acc. Chem. Res.*, 2018, **51**, 2465–2474; (*f*) R.-C. Jin, C.-J. Zeng, M. Zhou and Y.-X. Chen, *Chem. Rev.*, 2016, **116**, 10346–10413.

4 (*a*) X. Fan, F. R. Yuan, D. J. Li, S. Chen, Z. B. Cheng, Z. J. Zhang, S. C. Xiang, S.-Q. Zang, J. Zhang and L. Zhang, *Angew. Chem., Int. Ed.*, 2021, **60**, 12949–12954; (*b*) Y.-X. Du, H.-T. Sheng, D. Astruc and M.-Z. Zhu, *Chem. Rev.*, 2020, **120**, 526–622; (*c*) V. Sudheeshkumar, K. O. Sulaiman and R. W. J. Scott, *Nanoscale Adv.*, 2020, **2**, 55–69; (*d*) S. Maity, D. Bain and A. Patra, *Nanoscale*, 2019, **11**, 22685–22723; (*e*) Y.-M. Su, Z. Wang, C.-H. Tung, D. Sun and S. Schein, *J. Am. Chem. Soc.*, 2021, **143**, 13235–13244.

5 M.-M. Zhang, X.-Y. Dong, Z.-Y. Wang, X.-M. Luo, J.-H. Huang, S.-Q. Zang and T. C. W. Mak, *J. Am. Chem. Soc.*, 2021, **143**(16), 6048–6053.

6 Z. Wang, H.-T. Sun, M. Kurmoo, Q.-Y. Liu, G.-L. Zhuang, Q.-Q. Zhao, X.-P. Wang, C.-H. Tung and D. Sun, *Chem. Sci.*, 2019, **10**, 4862–4867.

7 (*a*) X.-Y. Li, H.-F. Su, K. Yu, Y.-Z. Tan, X.-P. Wang, Y.-Q. Zhao, D. Sun and L.-S. Zheng, *Nanoscale*, 2015, **7**, 8284–8288; (*b*) G. Li, Z. Lei and Q.-M. Wang, *J. Am. Chem. Soc.*, 2010, **132**, 17678–17679; (*c*) H. Y. Yang, J. Lei, B. H. Wu, Y. Wang, M. Zhou, A. D. Xia, L. S. Zheng and N. F. Zheng, *Chem. Commun.*, 2013, **49**, 300–302.

8 (*a*) X. Kang and M.-Z. Zhu, *Chem. Soc. Rev.*, 2019, **48**, 2422–2457; (*b*) Y.-P. Xie, Y.-L. Shen, G.-X. Duan, J. Han, L.-P. Zhang and X. Lu, *Mater. Chem. Front.*, 2020, **4**, 2205–2222.

9 (*a*) W.-M. He, Z. Zhou, Z. Han, S. Li, Z. Zhou, L.-F. Ma and S.-Q. Zang, *Angew. Chem., Int. Ed.*, 2021, **60**, 8505–8509; (*b*) R.-W. Huang, Y.-S. Wei, X.-Y. Dong, X.-H. Wu, C.-X. Du, S.-Q. Zang and T. C. W. Mak, *Nat. Chem.*, 2017, **9**, 689–697; (*c*) X.-Y. Li, Z. Wang, H.-F. Su, S. Feng, M. Kurmoo, C.-H. Tung, D. Sun and L.-S. Zheng, *Nanoscale*, 2017, **9**, 3601–3608.

10 (*a*) X.-H. Wu, P. Luo, Z. Wei, Y.-Y. Li, R.-W. Huang, X.-Y. Dong, K. Li, S.-Q. Zang and B.-Z. Tang, *Adv. Sci.*, 2019, **6**, 1801304; (*b*) Z.-C. Xie, P.-P. Sun, Z. Wang, H.-G. Li, L.-Y. Yu, D. Sun, M.-J. Chen, Y.-T. Bi, X. Xin and J.-C. Hao, *Angew. Chem., Int. Ed.*, 2020, **59**, 9922–9927.

11 (*a*) Y.-L. Shen, J.-L. Jin, J.-J. Fang, Z. Liu, J.-L. Shi, Y.-P. Xie and X. Lu, *Inorg. Chem.*, 2021, **60**, 6276–6282; (*b*) Q.-S. Wu, F. Bigdeli, F. Rouhani, X.-M. Gao, H. Kaviani, H.-J. Li, W. Wang, K.-G. Liu, M.-L. Hu, Xi.-Q. Cai and A. Morsali, *Inorg. Chem.*, 2021, **60**, 1523–1532.

12 C.-Y. Song, D.-F. Chai, R.-R. Zhang, H. Liu, Y.-F. Qiu, H.-D. Guo and G.-G. Gao, *Dalton Trans.*, 2015, **44**, 3997–4002.

13 H.-B. Wu, Z.-J. Huang and Q.-M. Wang, *Chem.–Eur. J.*, 2010, **16**, 12321–12323.

14 S.-S. Zhang, H.-F. Su, G.-L. Zhuang, X.-P. Wang, C.-H. Tung, D. Sun and L.-S. Zheng, *Chem. Commun.*, 2018, **54**, 11905–11908.

15 (*a*) H. W. Hou, Y. L. Wei, Y. L. Song, L. W. Mi, M. S. Tang and L. K. Li, *Angew. Chem., Int. Ed.*, 2005, **44**, 6067–6074; (*b*) W. F. Sun, M. M. Bader and T. Carvalho, *Opt. Commun.*, 2003, **215**, 185–190; (*c*) S. Vagin, M. Barthel, D. Dini and M. Hanack, *Inorg. Chem.*, 2003, **42**, 2683–2694.

16 (*a*) W. B. Lin, Z. Y. Wang and L. Ma, *J. Am. Chem. Soc.*, 1999, **121**, 11249–11250; (*b*) H. Chao, R.-H. Li, B.-H. Ye, H. Li, X.-L. Feng and J.-W. Cai, *J. Chem. Soc., Dalton Trans.*, 1999, 3711–3717.

17 H. W. Hou, X. R. Meng, Y. L. Song, Y. T. Fan, Y. Zhu and H. J. Lu, *Inorg. Chem.*, 2002, **41**, 4068–4075.

18 S. Shi, W. Ji, S. H. Tang, J. P. Lang and X. Q. Xin, *J. Am. Chem. Soc.*, 1994, **116**, 3615–3616.

19 (*a*) Y. Xu, C. Xu, T. Zhou and C. Cheng, *J. Mol. Struct.: THEOCHEM*, 2009, **893**, 88–92; (*b*) K. Zhou, C. Qin, L.-K. Yan, W.-E. Li, X.-L. Wang, H.-N. Wang, K.-Z. Shao and Z.-M. Su, *Dyes Pigm.*, 2015, **113**, 299–306; (*c*) Y. Chang, W. Q. Li and Y. Y. Jiang, *Phys. Lett. A*, 2012, **376**, 2314–2318.

20 (*a*) S. A. Khan, D. Senapati, T. Senapati, P. Bonifassi, Z. Fan, A. K. Singh, A. Neeley, G. Hill and P. C. Ray, *Chem. Phys. Lett.*, 2011, **512**, 92–95; (*b*) R. L. M. Gieseking, *Chem. Mater.*, 2019, **31**, 6850–6859.

21 (*a*) B. K. Teo and Y. H. Xu, *Inorg. Chem.*, 2001, **40**, 6794–6801; (*b*) J. F. Zhang, S. C. Meng, Y. L. Song, J. Y. Yang, H. Y. Wei, W. J. Huang, M. P. Cifuentes, M. G. Humphrey and C. Zhang, *New J. Chem.*, 2011, **35**, 328–338; (*c*) U. R. Felscia, B. J. M. Rajkumar, M. Nidya and P. Sankar, *J. Phys. Chem. A*, 2018, **122**, 1045–1052.

22 (*a*) A. Banerjee, T. K. Ghanty, A. Chakrabarti and C. Kamal, *J. Phys. Chem. C*, 2012, **116**, 193–200; (*b*) K. B. Bhavitha, A. K. Nair, S. Perumbilavil, S. Joseph, M. S. Kala, A. Saha, R. A. Narayanan, N. Hameed, S. Thomas, O. S. Oluwafemi and N. Kalarikkal, *Opt. Mater.*, 2017, **73**, 695e705; (*c*) U. R. Felscia and B. J. M. Rajkumar, *Mater. Lett.*, 2018, **221**, 318–321.

23 (*a*) R. Zhang, Y. Liu, L. Kong and X.-Y. Xu, *Spectrochim. Acta, Part A*, 2019, **223**, 117338; (*b*) X. Chen, J. Tao, G. Zou, W. Su, Q. J. Zhang and P. Wang, *ChemPhysChem*, 2010, **11**, 3599–3603; (*c*) J. H. Li, J. F. Zhang, M. G. Humphrey and C. Zhang, *Eur. J. Inorg. Chem.*, 2013, 328–346.

24 K. Zhou, Y. Geng, L.-K. Yan, X.-L. Wang, X.-C. Liu, G.-G. Shan, K.-Z. Shao, Z.-M. Su and Y.-N. Yu, *Chem. Commun.*, 2014, **50**, 11934–11937.
25 (*a*) M.-L. Chen, X.-F. Xu, Z.-X. Cao and Q.-M. Wang, *Inorg. Chem.*, 2008, **47**, 1877–1879; (*b*) M.-X. Yang, L.-J. Chen, S. Lin, X.-H. Chen and H. Huang, *Dalton Trans.*, 2011, **40**, 1866–1872.
26 (*a*) V. Bonačić-Koutecký and R. Antoine, *Nanoscale*, 2019, **11**, 12436–12448; (*b*) I. Russier-Antoine, F. Bertorelle, N. Calin, Ž. Sanader, M. Krstić, C. Comby-Zerbino, P. Dugourd, P.-F. Brevet, V. Bonačić-Koutecký and R. Antoine, *Nanoscale*, 2017, **9**, 1221–1228; (*c*) B. Bhushan, T. Kundu and B. P. Singh, *Opt. Commun.*, 2012, **285**, 5420–5424.
27 M. Sheik-Bahae, A. Said, T.-H. Wei, D. J. Hagan and E. W. Van Stryland, *IEEE J. Quantum Electron.*, 1990, **26**, 760–769.
28 P. B. Chapple, J. Staromlynska, J. A. Hermann and T. J. Mckay, *J. Nonlinear Opt. Phys. Mater.*, 1997, **6**, 251–293.
29 K. Mashima, M. Tanaka, Y. Kaneda, A. Fukumoto, H. Mizomoto and K. Tani, *Chem. Lett.*, 1997, 411–412.
30 (*a*) H. El Ouazzani, K. Iliopoulos, M. Pranaitis, O. Krupka, V. Smokal, A. Kolendo and B. Sahraoui, *J. Phys. Chem. B*, 2011, **115**, 1944–1949; (*b*) H.-T. Shi, L.-J. Zhou, A.-Q. Jia, Q. Chen and Q.-F. Zhang, *J. Coord. Chem.*, 2013, **66**, 3740–3748.
31 K. Iliopoulos, A. El-Ghayoury, H. El Ouazzani, M. Pranaitis, E. Belhadj, E. Ripaud, M. Mazari, M. Sallé, D. Gindre and B. Sahraoui, *Opt. Express*, 2012, **20**, 25311–25316.
32 (*a*) Z. G. Xiao, J. F. Ge, R. Sun, Y. Fang, Y. C. She, Z. G. Li, X. Z. Wu, S. Liu, L. Li, Y. J. Jian and Y. L. Song, *Opt. Mater.*, 2018, **83**, 300–305; (*b*) Z. G. Xiao, J. F. Ge, Z. G. Li, X. Z. Wu, Y. Fang, G. Shi, X. R. Zhang, Y. X. Wang and Y. L. Song, *Opt. Mater.*, 2015, **50**, 263–267.
33 (*a*) B. Cichy, D. Wawrzynczyk, M. Samoc and W. Stręk, *J. Mater. Chem. C*, 2017, **5**, 149–158; (*b*) J.-H. Jia, X.-M. Tao, Y.-J. Li, W.-J. Sheng, L. Han, J.-R. Gao and Y.-F. Zheng, *Chem. Phys. Lett.*, 2011, **514**, 114–118.
34 Z. G. Li, F. Gao, Z. G. Xiao, G. D. Ao, X. Z. Wu, Y. Fang, Z. Q. Nie, T.-H. Wei, J. Y. Yang, Y. X. Wang, X. R. Zhang, J. L. Zuo and Y. L. Song, *Dyes Pigm.*, 2015, **119**, 70e74.
35 T. Lu and F. W. Chen, *J. Comput. Chem.*, 2012, **33**, 580–592.
36 G. M. Chu, I. Fernández and M. A. Sierra, *Chem.–Eur. J.*, 2013, **19**, 5899–5909.